Patterns of phase-dependent spiral wave attenuation in excitable media

M. A. de la Casa,[1] F. J. de la Rubia,[1] and Plamen Ch. Ivanov[2,3]
[1]*Departamento Física Fundamental, Universidad Nacional de Educación a Distancia, c/ Senda del Rey 9,28080 Madrid, Spain*
[2]*Center for Polymer Studies and Department of Physics, Boston University, Boston, Massachusetts 02215, USA*
[3]*Harvard Medical School, Division of Sleep Medicine, Brigham and Women's Hospital, Boston, MA 02115, USA*
(Received 28 February 2006; revised manuscript received 7 December 2006; published 30 May 2007)

We show that introducing periodic planar fronts with long excitation duration can lead to spiral attenuation. The attenuation occurs periodically over cycles of several planar fronts, forming a variety of complex spatiotemporal patterns. We find that these attenuation patterns occur only at specific phases of the descending fronts relative to the rotational phase of the spiral. These patterns fall into two general classes, each defined by a specific expression for the number of attenuated spirals per cycle of planar fronts, and represented by a structured diagram in parameter space. The spiral attenuation patterns we observe remain stable in time and do not change during the evolution of the system.

DOI: 10.1103/PhysRevE.75.051923 PACS number(s): 87.18.Bb, 87.19.Hh, 89.75.Kd, 87.18.Hf

Spiral waves underlie mechanisms related to a wide spectrum of phenomena, ranging from spatially extended chemical reactions to fatal cardiac arrythmias [1–7]. Different approaches to prevent spiral breakup have been proposed [8–12]. Here, we focus on the attenuation of a single stable spiral wave. It has been shown that pulses with frequency higher than the spiral frequency can eliminate spiral waves by forcing them to drift off the medium [13,14], since the highest-frequency domain pervades the medium [15–19]. We show that it is possible to attenuate stable spiral waves by planar wave fronts with period longer than the rotational period of the spiral, and we address the problem of how to control spiral attenuation in excitable media. We find that, when the fronts have long excitation duration, and are delivered at a specific phase relative to the rotational phase of the spiral, the spiral-front interaction is characterized by periodic patterns of spiral attenuation, which remain stable in time, and are observed for a broad range of physiologically meaningful parameter values.

We perform numerical simulations on a two-dimensional (2D) square lattice by considering the interactions between the cells in the lattice based on physiologically motivated rules, representing the excitation dynamics of myocardial cells. In the model, the transmembrane potential of a myocardial cell represents the state of excitation of that cell. We model the state of the cell in position (i,j) in the lattice by an integer number E_{ij} as follows. (i) *Resting (equilibrium) state:* This state is represented in our model by $E_{ij}=0$, which corresponds to the experimentally observed transmembrane potential ≈ -90 mV. A cell remains in the resting state for an unlimited time until a superthreshold perturbation occurs in the medium, which brings the cell to the excited state. This threshold for ventricular cells in guinea pigs was experimentally found to be $\approx 4-8$ V/cm [20], and is represented in our model by the parameter $\mathcal{T}_{rest}$. (ii) *Excited state:* When a cell enters the excited state, it takes a value in the interval $E_{min} \leqslant E_{ij} \leqslant E_{max}$, where $E_{min}>1$. For an excited cell, in every time step τ, E_{ij} decreases by 1. Thus, in our simulations E_{ij} not only represents the transmembrane potential but also has the meaning of excitation duration, where at the beginning of the excitation the lowest excitation level a cell can assume is E_{min}, corresponding to the shortest possible action potential duration (APD), while the highest excitation level is E_{max}, which corresponds to the longest APD. At the end of the excitation period, $E_{ij}=1$ before the cell becomes absolute refractory. (iii) *Absolute refractory state:* When a cell enters this state, E_{ij} falls to $-R_a-R_r$, where R_a is the duration of the absolute refractory state when a cell cannot be excited. For an absolutely refractory cell, in every time step τ, E_{ij} increases by 1. After R_a time steps the cell becomes relatively refractory (at $E_{ij}=-R_r$) before it reaches the resting state. (iv) *Relative refractory state:* This state is represented by $-R_r \leqslant E_{ij} \leqslant -1$, where R_r is the duration of the relative refractory state. A cell in this state can be excited with an excitation threshold experimentally observed to decrease in time as the cell approaches the resting state [21]. This threshold remains higher than the threshold of cells in the resting state [21], and in our model, it decreases linearly in time from the value $\mathcal{T}_{rest}$, when $E_{ij}=-R_r$, to the value $\mathcal{T}_{ref}$ in the resting state. For every time step τ in which a relatively refractory cell does not become excited, E_{ij} is increased by 1, until the cell reaches the resting state $E_{ij}=0$.

We define the excitation stimulus received by a cell in position (i,j) from the neighboring cells as $S_{ij}=\Sigma_{k,l}W_{kl}\sigma_{kl}$, where $k \in [i-\epsilon, i+\epsilon]$, $l \in [j-\epsilon, j+\epsilon]$, and ϵ defines the range of interaction. W_{kl} is a rotationally symmetric interaction kernel as defined in [22], and $\sigma_{kl}=1$ if the cell in position (k,l) is excited and $\sigma_{kl}=0$ otherwise. To preserve a proper relation between the speed of propagation and the curvature of the wave front, we set $\epsilon=5$. To account for the weaker effects of more distant neighbors, we choose values of the kernel elements W_{kl} decreasing with increasing distance from the center of the kernel [22]. In our simulations, a cell in position (i,j) that is excitable at time t will become excited in the next time step $t+1$ if it receives a stimulus S_{ij} larger than the excitation threshold of the cell. In this case, the new excited state of the cell is given by $E_{ij}^{t+1}=E_{ij}^{t}+R_r+E_{min}$, so that a cell at the beginning of the relative refractory state, with $E_{ij}^{t}=-R_r$, will reach an excitation level $E_{ij}^{t+1}=E_{min}$. This is in accordance with the experimentally observed behavior of the restitution curve [23]. To account for the ion leakage from excited neighboring cells, we allow for an excitable cell to

TABLE I. Parameter values used in our simulations. R, refractory period; R_r, relative refractory period; E_{max}, maximum APD; E_{min}, minimum APD; $\mathcal{T}_{ref}$, excitation threshold at the beginning of the relative refractory period; $\mathcal{T}_{rest}$, excitation threshold in the resting state. R, R_a, E_{max}, and E_{min} are given in terms of the time unit τ, while the excitation threshold is given in arbitrary units.

Parameter	Value
R	18–30
R_r	7–10
E_{max}	10–20
E_{min}	2–4
$\mathcal{T}_{ref}$	48
$\mathcal{T}_{rest}$	20

reach the longest APD, $E_{ij}^{t+1}=E_{max}$, if simultaneously (i) we have a cell (k,l) included in the kernel that is in the state $E_{kl}^{t}=E_{max}$, and (ii) the perturbation S_{ij} is larger than the excitation threshold.

The values of the parameters and the rules in our model match well the excitation dynamics in the ventricular cells of the guinea pig, traditionally used in experimental settings and theoretical studies [23]. (a) The experimentally observed excitable gap (the time between the end of the absolute refractory period and the next excitation) is $G=12\pm4$ ms [23], which corresponds to one time step τ in our simulations, so we have $\tau=12$ ms. (b) Comparing the experimental propagation speed of $v\approx75$ cm/s [23] with the wave propagation of three lattice cells per time unit τ in our model, we have that our spatial unit is $\delta=0.3$ cm (≈100 myocite cells). (c) The experimentally found refractory period $R^{expt}\equiv R_a^{expt}+R_r^{expt}\approx200$ ms, and relative refractory period $R_r^{expt}\approx120$ ms [23] are approximated in our simulation by the parameter values $R\equiv R_a+R_r\in[18,30]$ and $R_r\in[7,10]$, in units of the time step τ. (d) The minimum and maximum APDs experimentally observed are $E_{min}^{expt}\approx40$ ms and $E_{max}^{expt}\approx160$ ms [23], which correspond to our parameters $E_{min}\in[2,4]$ and $E_{max}\in[10,20]$, in units of the time step τ. (e) The prolongation of the APD due to ion leakage has been physiologically estimated as $\Delta(\mathrm{APD})^{expt}\approx D(\mathrm{APD})\partial_{xx}(\mathrm{APD})$, where $D\approx1$ cm^2/s is a diffusion constant. Since typically APD $\approx(E_{max}^{expt}+E_{min}^{expt})/2$ and $\partial_{xx}(\mathrm{APD})\approx(E_{max}^{expt}-E_{min}^{expt})/\delta^2$, we find $\Delta(\mathrm{APD})^{expt}\approx130$ ms which compares to the maximum prolongation in our model $\Delta(\mathrm{APD})^{model}=E_{max}-E_{min}\in[6,18]$ in units of τ. The shape of the model restitution curve mimics the experimental data [23] (see Fig. 1). Thus, our model is based on experimentally relevant parameter values. Table I gives all the model parameters and the values used in our simulations.

We generate the spiral according to a standard procedure [24]. When the spiral reaches a stable rotation (after 300 time steps τ, i.e., ≈15 spiral rotations), we introduce planar fronts with a period T starting from the edge of the lattice, each generated as a single line of excited cells with maximum APD, $E_{1j}=E_{max}$, for $j=1,\ldots,N$. We release the first front at time T_0 (in units of τ) after the stabilization period of the spiral. The width of the front is proportional to the parameter

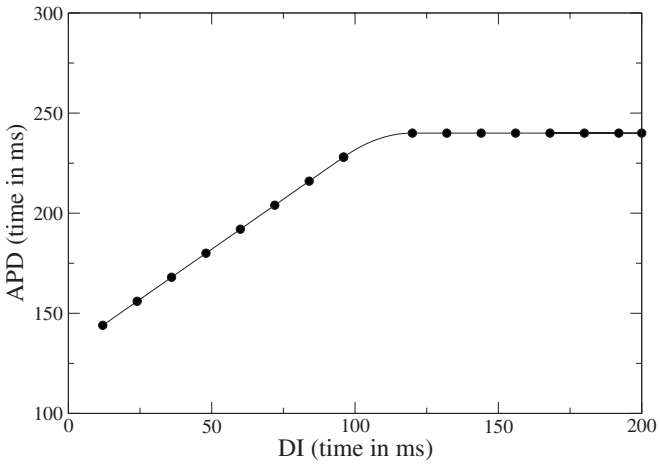

FIG. 1. Model restitution curve. The action potential duration (APD) is the duration of the excited plus absolute refractory states and is plotted versus the diastolic interval (DI), i.e., the time since the end of the last action potential to the next excitation event. In this plot, $E_{min}=2$, $E_{max}=10$, $R_a=10$, and $R_r=8$. The positive slope region is the relative refractory state, and the flat region is the resting state.

E_{max} and to the speed of propagation, which depends on the excitation thresholds $\mathcal{T}_{rest}$ and $\mathcal{T}_{ref}$. Under these conditions, the position of the spiral tip remains within a very small area (≈30 cells) and the observed patterns of spiral attenuation are not the result of spiral drift. To avoid effects of the lattice edge on the dynamics of wave propagation, and to account for experimental settings [25] we introduce no-flux boundary conditions. To track if the spiral is attenuated, we follow the time evolution of every individual cell in the lattice. To survey the system, we also measure the total number of excited cells in the lattice as a function of time.

We find that the interaction between the fronts and the spiral leads to complex patterns where, after several passing fronts, the spiral is attenuated (Fig. 2). These patterns repeat in time and remain stable for a broad range of parameter values (Fig. 4). Further, we find that all different patterns fall into two general classes: (i) Class I, where there is one spiral attenuation within a cycle of several passing fronts [Figs. 2(a)–2(c)], and (ii) Class II, where there are two nonconsecutive spiral attenuations within a cycle of several passing fronts [Figs. 2(d)–2(f)]. Repeating our simulations for $N\times N$ and $N\times2N$ lattices with $N=60,80,100,\ldots,200$, we find identical dynamics with the same periodic patterns of spiral attenuation.

In our simulations the APD of a cell that becomes excited is $E_{ij}^{t+1}=E_{ij}^{t}+R_r+E_{min}$. Since the excitable gap in experimental settings is $G\approx12$ ms [23], which corresponds to one time step τ in our simulations, a cell in the relative refractory state $E_{ij}^{t}=-R_r$ is excited within a single time step to $E_{ij}^{t+1}=E_{min}$. Thus, the APD of a cell in the isolated spiral is always E_{min}. Therefore, the restitution curve has a positive constant slope during the relative refractory period, followed by a plateau during the resting state (Fig. 1). The patterns of spiral attenuation we present in Fig. 2 are a result of a complex nonlinear interaction between the spiral and the descending fronts. Without the fronts, the rotational period of the spiral is uni-

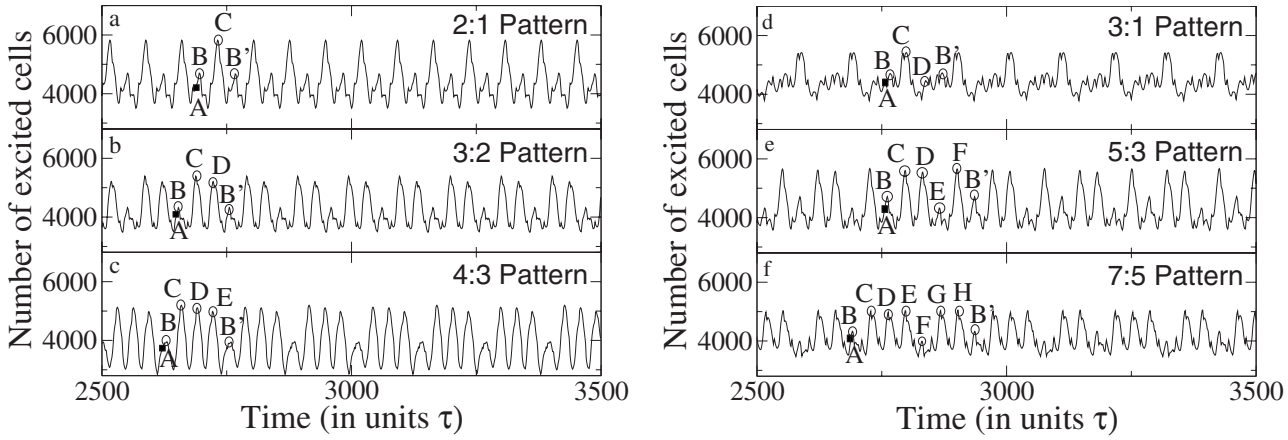

FIG. 2. Time evolution of the total number of excited cells on a square lattice of size $N=100$, showing the two classes of spiral attenuation patterns. Absent and reduced peaks correspond to attenuation of the spiral. For Class I $(n:n-1)$ patterns, within a cycle of n fronts we have $n-1$ consecutive spiral rotations followed by one spiral attenuation: (a) pattern 2:1—out of the collision of the spiral with two consecutive fronts there is first a spiral attenuation (denoted by B) followed by one surviving spiral (denoted by C); (b) pattern 3:2—for each cycle of three consecutive fronts there is first a spiral attenuation (B) followed by two surviving spirals (C and D); (c) pattern 4:3—for each cycle of four consecutive fronts there is a spiral attenuation (B) and three surviving spirals (C, D, and E). The Class I patterns in (a), (b), and (c) are obtained for the parameter values $R_a=16$, $R_r=8$, $E_{min}=2$, $E_{max}=17,15,13$, $T_0=73,39,64$, respectively. For Class II $(2n+1:2n-1)$ patterns, within a cycle of $2n+1$ fronts there are $2n-1$ spiral rotations and two spiral attenuations: (d) pattern 3:1—for each cycle of three fronts there are two spiral attenuations (B and D) and one surviving spiral (C); (e) pattern 5:3—for each five fronts there are two spiral attenuations (B and E) and three surviving spirals (C, D, and F); (f) pattern 7:5—for each seven fronts we have two attenuations (B and F) and five surviving spirals (C, D, E, G, and H). The Class II patterns in (d), (e), and (f) are obtained for the parameter values $R_a=15,16,17$, $R_r=8$, $E_{min}=2$, $E_{max}=17,16,15$, $T_0=65,70,70$, respectively. In all panels, the instant in which a spiral attenuation is initiated is denoted by A, and the beginning of the next cycle is denoted by B'. We choose $\mathcal{T}_{rest}=20$ and $\mathcal{T}_{ref}=48$ to maintain the movement of the spiral tip in our simulations in an area of ≈30 cells, in agreement with experimental observations [23].

form in both space and time, i.e., the excitation of every cell in the lattice has a period equal to the rotational period of the spiral. The period of the spiral is defined as the sum of the duration of all states a cell undergoes during a single spiral rotation, $T_{sp}^{-}=E_{min}+R_a+G$. In the presence of fronts, where the excited cells have maximum APD given by $E_{ij}=E_{max}$, after a collision of a front with the spiral, a thin layer of maximum APD excitations propagates from the front along the advancing contour of the spiral (as shown in Fig. 3, frames 2–4). When these excitations reach the tip of the spiral before the next spiral rotation, the period of the spiral increases to $T_{sp}^{+}=E_{max}+R_a+G$, which is also the period of the cells with maximum APD. In this case, the spiral survives and we observe a peak in the total number of excited cells in the lattice (Fig. 2). When the layer of cells with maximum APD excitations, which propagates from the front to the spiral, does not reach the tip of the spiral before the next spiral rotation (i.e., it does not cover the entire contour of the spi-

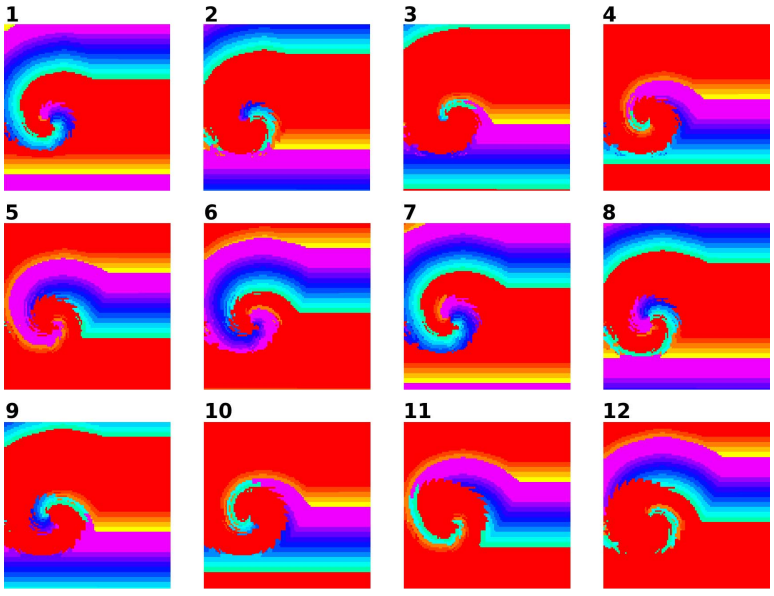

FIG. 3. (Color online) Color-coded representation of the time evolution for the Class I 4:3 pattern obtained for the same parameter values as in Fig. 2(c). Snapshots represent the state of the lattice at intervals of five time steps τ. Snapshots 1, 7, and 12 correspond to D, E, and A in Fig. 2(c). In the first snapshot, the central region is refractory, with a planar front being introduced from below, while the upper part of the frame is covered by the spiral. Absolute refractory cells are in red, relative refractory cells in orange and yellow, and excited cells in shades of blue and violet in the online version.

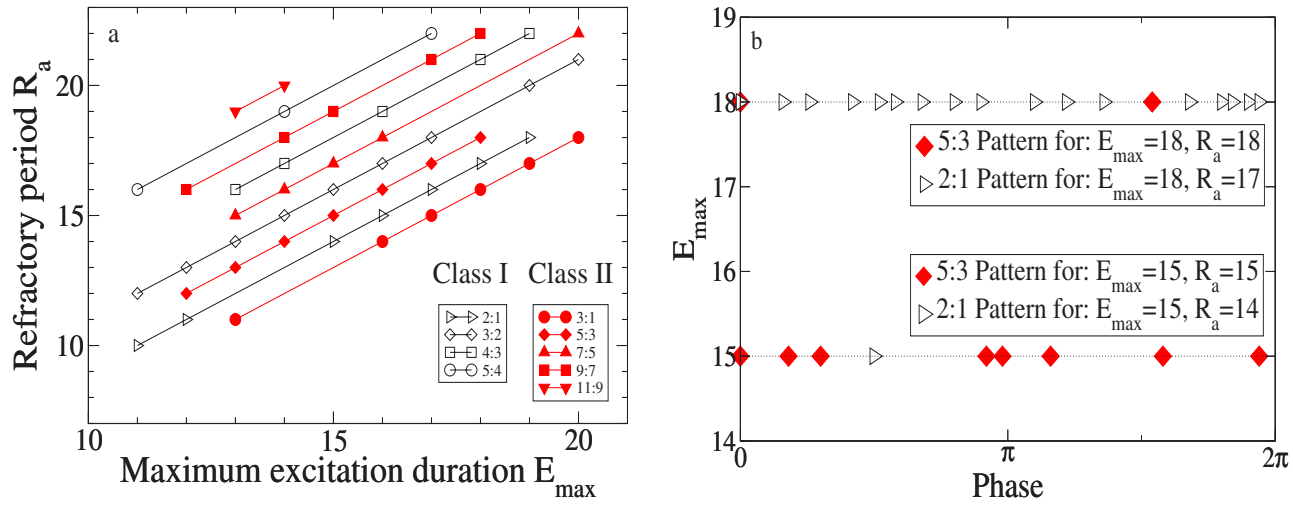

FIG. 4. (Color online) (a) Pattern diagram in parameter space R_a versus E_{max}, for a square lattice of $N=100$ and fixed parameter values $R_r=8$ and $E_{min}=2$. We observe attenuation patterns for a broad range of parameter values where each pattern can be found along a single straight line, in accordance with Eqs. (2) and (4). Patterns of Class I and Class II alternate in a series of parallel lines, where n increases with increasing R_a. Empty symbols represent Class I patterns, while solid symbols represent Class II patterns. (b) Dependence of the attenuation patterns on the relative phase between the first released front and the spiral. Presented are only the patterns 2:1 (Class I) and 5:3 (Class II) for two sets of parameter values E_{max} and R_a, with the same symbols as in (a). For each set of parameter values, the patterns in (a) can appear only for specific relative phases, indicating that the phase in which the front hits the spiral is crucial to achieve spiral attenuation.

ral), the period of the spiral remains T_{sp}^-. In this case, the cells at the tip of the spiral continue to have short APD given by $E_{ij}=E_{min}$ (Fig. 3, frame 11). Due to the short APD, the spiral cannot propagate through the absolutely refractory areas left by the layer of cells with long APD (given by $E_{ij}=E_{max}$) formed between the front and the spiral, and the spiral is attenuated (Fig. 3, frame 12). This spiral attenuation corresponds to a reduced, or absent, peak in the total number of excited cells (Fig. 2). In our simulations, $T=T_{sp}^++2$. Thus, the spiral attenuation we observe (Figs. 1 and 2) is achieved for planar fronts with a period lower than the period of the spiral.

The patterns we show in Figs. 2 and 3 cannot be matched by a linear superposition of the number of excited cells in the isolated spiral and the isolated fronts. Such linear superposition exhibits periodic pulses with a much higher number of excited cells and cannot account for the missing peaks associated with spiral attenuation. The number of excited cells during spiral attenuation (frame 12 in Fig. 3) is greatly decreased compared to that of the spiral alone (frame 6 in Fig. 3).

For Class I $(n:n-1)$ patterns, we observe that, within a cycle of n fronts, we have $n-1$ slow spiral rotations with period T_{sp}^+, followed by two fast rotations with period T_{sp}^-:

$$nT=(n-1)T_{sp}^++2T_{sp}^-, \quad \text{class I}, \tag{1}$$

where the two fast rotations correspond to a single episode of spiral attenuation. Solving for n in Eq. (1), we obtain

$$n=\frac{4T_{sp}^--2T_{sp}^+}{2(T-T_{sp}^+)}=\frac{1}{2}(2E_{min}-E_{max}+R_a+G). \tag{2}$$

For Class II $(2n+1:2n-1)$ patterns, we observe that, within a cycle of $2n+1$ fronts, we have $2n-1$ slow spiral rotations, with period T_{sp}^+, and four fast rotations, with period T_{sp}^-:

$$(2n+1)T=(2n-1)T_{sp}^++4T_{sp}^-, \quad \text{class II}, \tag{3}$$

where the four fast rotations correspond to two separate nonconsecutive episodes of spiral attenuation. Solving for n in Eq. (3), we obtain

$$n=\frac{4T_{sp}^--T_{sp}^+-T}{2(T-T_{sp}^+)}=\frac{1}{2}(2E_{min}-E_{max}+R_a+G-1). \tag{4}$$

Based on the choice of parameter values for the system, the above expressions allow us to predict (i) the specific attenuation pattern, and (ii) the class to which a given pattern belongs. Parameter values for which we do not obtain integer n in either Eq. (2) or Eq. (4) cannot lead to spiral attenuation patterns. Thus, we can control the dynamical behavior of the system in generating desired patterns of spiral attenuation.

Our simulations of up to 10^5 time steps τ (corresponding to $\approx$1500 s in experimental settings) show no change in the dynamics, which indicates that the spiral attenuation patterns remain stable in time. Further, we find that both Class I and Class II patterns can be obtained for a broad range of parameter values showing a robust effect of spiral attenuation. Specifically, we observe a particular structure in parameter space where individual patterns are organized along parallel straight lines, with every even line corresponding to a Class I pattern and every odd line corresponding to a Class II pattern [Fig. 4(a)]. This regular structure in parameter space is also predicted by Eqs. (2) and (4). In the upper left corner of the parameter diagram, for increasing values of R_a and decreasing values of E_{max}, since we have one attenuation per cycle of n fronts for Class I patterns, and two attenuations per cycle for $2n+1$ fronts for Class II, as expected, an at-

tenuation becomes less frequent for increasing n. In the upper right (large R_a and E_{max}) and lower left (small R_a and E_{max}) corners of the diagram, we find alternating patterns in a broad range of parameter values extending beyond the physiologically meaningful region [not shown on the diagram in Fig. 4(a)]. Finally, in the lower right corner of the diagram (small R_a and large E_{max}) we do not observe patterns. This is in agreement with Eqs. (2) and (4), which do not allow $n < 2$ for Class I (a cycle of at least two fronts is needed to have one attenuation within the cycle), and $n < 1$ for Class II (a cycle of at least three fronts is needed to have two attenuations within the cycle).

Finally, we investigate how the front-spiral interaction depends on the relative phase between the spiral and the fronts. To answer this question, we perform several tests by releasing the first front at a time T_0 after the stabilization period of the spiral, followed by a train of fronts with period T. We repeat the simulations for every value of $T_0 \in [0,T]$, for every point in the parameter space shown in Fig. 4(a). Surprisingly, we find that the patterns we observe in the parameter diagram of Fig. 4 occur only for specific values of T_0. For example, the Class I 2:1 pattern generated for $E_{max}=15$ and $R_a=14$ occurs only for phase $2\pi/4$, corresponding to $T_0 = T/4$, while the same pattern, for $E_{max}=18$ and $R_a=17$, occurs for several values of T_0 [Fig. 4(b)]. Thus, the observed dynamical patterns of spiral attenuation shown in Fig. 2 depend not only on the parameter values, but also on the specific values of the relative phase between the spiral wave and the first released front. These findings indicate the presence of particular "vulnerable" phases during the spiral rotation when planar fronts can lead to spiral attenuation patterns. While our model is relatively simple and takes into account only the basic elements of the excitable dynamics, it is also very general, and, therefore, the results we obtain could be of relevance to single spiral cardiac arrhythmias such as monomorphic ventricular tachycardia.

Miguel A. de la Casa and Javier de la Rubia acknowledge partial support by the Ministerio de Educación y Ciencia (Spain), Project No. FIS2005–01729, and Plamen Ch. Ivanov acknowledges support from NIH Grant No. 2R01 HL071972.

[1] A. T. Winfree, Science **175**, 634 (1972).
[2] F. Siegert and C. J. Weijer, J. Cell. Sci. **93**, 325 (1989).
[3] S. Jakubith, H. H. Rutermund, W. Engel, A. von Overtezen, and G. Ertl, Phys. Rev. Lett. **65**, 3013 (1990).
[4] J. M. Davidenko *et al.*, Nature (London) **355**, 349 (1992).
[5] R. A. Gray *et al.*, Science **270**, 1222 (1995).
[6] F. X. Witkowski *et al.*, Nature (London) **392**, 78 (1998).
[7] H. M. Hastings *et al.*, Proc. Natl. Acad. Sci. U.S.A. **93**, 10495 (1996).
[8] V. Petrov *et al.*, Nature (London) **361**, 240 (1993).
[9] V. S. Zykov, A. S. Mikhailov and S. C. Muller, Phys. Rev. Lett. **78**, 3398 (1997).
[10] W. L. Ditto *et al.*, Int. J. Bifurcation Chaos Appl. Sci. Eng. **10**, 593 (2000).
[11] S. Sinha, A. Pande, and R. Pandit, Phys. Rev. Lett. **86**, 3678 (2001).
[12] M. Woltering and M. Markus, Phys. Lett. A **297**, 363 (2002).
[13] H. Sakaguchi and Y. Kido, Phys. Rev. E **71**, 052901 (2005).
[14] A. V. Panfilov, S. C. Muller, V. S. Zykov, and J. P. Keener, Phys. Rev. E **61**, 4644 (2000).
[15] A. N. Zaikin and A. M. Zhabotinsky, Nature (London) **225**, 535 (1970).
[16] A. T. Stamp *et al.*, Chaos **12**, 931 (2002).
[17] I. Aranson, H. Levine, and L. Tsimring, Phys. Rev. Lett. **76**, 1170 (1996).
[18] K. J. Lee, Phys. Rev. Lett. **79**, 2907 (1997).
[19] F. Xie, Z. Qu, J. Weiss, and A. Gartinkel, Phys. Rev. E **59**, 2203 (1999).
[20] V. Sharma *et al.*, Biophys. J. **88**, 3038 (2005).
[21] *Essential Medical Physiology*, edited by L. R. Johnson (Lippincott-Raven, Philadelphia, 1998).
[22] V. G. Fast *et al.*, Phys. Lett. A **151**, 157 (1990).
[23] S. D. Girouard *et al.*, Circulation **93**, 603 (1996).
[24] V. N. Biktashev and A. V. Holden, Chaos **8**, 48 (1998).
[25] J. M. Starobin and C. F. Starmer, Phys. Rev. E **54**, 430 (1996).